

Excitation and inhibition imbalance affects dynamical complexity through symmetries

Mathieu Ouellet,¹ Jason Z. Kim,² Harmange Guillaume,^{3,4} Sydney M. Shaffer,^{2,4,5} Lee C. Bassett,^{1,6} and Dani S. Bassett^{1,2,6,7,8,9,10}

¹*Department of Electrical & Systems Engineering, School of Engineering and Applied Science, University of Pennsylvania, Philadelphia, PA 19104 USA*

²*Department of Biological Engineering, School of Engineering & Applied Science, University of Pennsylvania, Philadelphia, PA 19104 USA*

³*Perelman School of Medicine, University of Pennsylvania, Philadelphia, PA, USA*

⁴*Cell and Molecular Biology Group, Perelman School of Medicine, University of Pennsylvania, Philadelphia, PA, USA*

⁵*Department of Pathology and Laboratory Medicine, Perelman School of Medicine, University of Pennsylvania, Philadelphia, PA, USA*

⁶*Co-contributors.*

⁷*Department of Physics & Astronomy, College of Arts & Sciences, University of Pennsylvania, Philadelphia, PA 19104 USA*

⁸*Department of Neurology, Perelman School of Medicine, University of Pennsylvania, Philadelphia, PA 19104 USA*

⁹*Department of Psychiatry, Perelman School of Medicine, University of Pennsylvania, Philadelphia, PA 19104 USA*

¹⁰*Santa Fe Institute, Santa Fe, NM 87501 USA**

(Dated: February 25, 2022)

From the perfect radial symmetries of radiolarian mineral skeletons to the broken symmetry of homochirality, the logic of Nature’s regularities has fascinated scientists for centuries. Some of Nature’s symmetries are clearly visible in morphology and physical structure, whereas others are hidden in the network of interactions among system components. Just as visible symmetries and asymmetries contribute to the system’s beauty, might hidden symmetries contribute to the system’s functional harmony? And if so, how? Here we demonstrate that the interaction networks of biological systems—from cell signaling to cancer—display a form of dynamical reflection symmetry that serves to expand their dynamical complexity. The expansion proceeds according to precise rules regarding the lengths of dynamical cycles, made possible by a peculiar imbalance between excitation and inhibition. To probe the conditions under which this reflection symmetry evolves, we use a multi-objective genetic algorithm to produce networks with long dynamical cycles. We find that local structural motifs that break the reflection symmetry are deleted in the evolutionary process, providing evidence for symmetry’s causal role in dynamical complexity. Finally, we identify symmetries in real continuous-valued scRNA-seq data of gene expression in cancer cells that is predictive of drug resistance. Broadly, our work reveals a class of hidden symmetries in biology, present in the network of interactions among system components, and it underscores their functional importance. Mathematically simple and computationally inexpensive, our approach is applicable to the types of biological data commonly acquired in modern experiments.

One of the most intriguing characteristics of complex systems is that they evince emergent global functions from local interactions. Gene regulatory networks are a quintessential example, describing the complex network of short time-scale interactions between molecules to produce the long time-scale cycles of reactions that sustain life [1–4]. Such cyclic behaviours play a fundamental role in many processes including cell cycles [5], biological clocks [6], cell fate [7], cancer regulation and DNA damage [8], and signaling [9]. Despite their significance, understanding the precise mechanism of emergence for long cyclic reactions is made difficult by the nonlinear and heterogeneous distribution of interactions. Can we distill simple principles for how specific patterns of local

interactions determine long and complex cycles of reactions?

To shed light on this question, biological systems have been fruitfully modeled as Boolean networks. In these models, the state of each component—a gene, protein, or RNA—is described by a binary value, and the interactions between components—binding, chemical reaction, and so on—are described by Boolean functions. Prior work has extensively studied the interaction functions [10–12] to model probabilistic [13] and multi-level [14] interactions, or to stabilize existing sequences of reactions [15]. Other work has focused on the intensive study of specific network topologies [2, 3, 16–19] and local structures that are typically referred to as motifs [20]. However, we still lack a general understanding of how the local interaction topology determines long sequences of cycles, thereby limiting our ability to make principled predictions across different networks about the global effects of local perturbations.

* To whom correspondence should be addressed: dsb@seas.upenn.edu

Here, we provide such an understanding through the analytical and numerical study of Boolean network topology. First, we use an evolutionary algorithm to optimize for network motifs with long cycle lengths, and discover the existence of *forbidden motifs* that are almost completely absent in the evolved networks. Next, we discover that many such evolved networks display a *dynamical reflection symmetry*, such that if the network at state x transitions to state y , then that same network at state $1 - x$ transitions to state $1 - y$. To bring these two results together, we analytically prove that a simple local rule—namely, that the incoming excitatory connections outnumber by one the incoming inhibitory connections at each node—is sufficient to produce this dynamical reflection symmetry; moreover, we find that the forbidden motifs systematically violate this condition.

To demonstrate the practical utility of our theory, we apply it to real biological systems, and find that reflection symmetry appears naturally in networks that have evolved to support long dynamical cycles, whereas forbidden motifs decrement the length of dynamical cycles. Further, we detect reflection symmetry in real continuous-valued scRNA-seq data of gene expression in cancer cells that is predictive of drug resistance, despite the fact that the full dynamical process underlying the system’s evolution remains unknown. Collectively, our findings serve to demonstrate how dynamical symmetries explain the observed complexity of biological systems.

BOOLEAN NETWORK MODEL

The state of biological systems generally—and gene regulatory systems specifically—can be simply represented by Boolean states (0,1) where 0 indicates low concentration or activity and 1 indicates high concentration or activity. Following the typical construction [14], our model consists of a set of n ordered nodes with a binary state represented by a Boolean vector $\vec{x}(t) = (x_1(t), x_2(t), \dots, x_n(t))$. For a given network, we refer to the set of 2^n states as the *state space* (see Figure 1.A). The nature of the state space is determined by two factors: the types of edges that connect nodes (see Figure 1.B), and the rules by which nodes update their states. We will discuss each in turn.

To guide the choice of edge type, we consider gene regulatory networks where coordinated interactions between the different nodes (genes, RNAs, proteins, and so on) cause each node’s state to fluctuate in time. Two main types of interactions—inhibitory and excitatory—control the pattern of node activity. Excitatory interactions increase gene expression or protein concentration, whereas inhibitory interactions decrease that expression or concentration. To reproduce these mechanisms, we allow edges to be excitatory or inhibitory. Excitatory edges take the value 1, and inhibitory edges take the value -1 . These values can be stored in a weighted adjacency matrix, \mathbf{A} , with elements A_{ij} representing the edge connect-

ing node j to node i .

The states of all nodes are updated in discrete time steps; all states are updated at once. At every time step, each node sums the excitatory and inhibitory inputs, and if that sum is greater than 0, then the node becomes active (1); otherwise it becomes inactive (0). The update rule can be formally specified as follows:

$$x_i(t+1) = \begin{cases} 1, & \text{if } \sum_j A_{ji}x_j(t) > 0 \\ 0, & \text{if } \sum_j A_{ji}x_j(t) \leq 0 \end{cases} \quad (1)$$

This threshold model is similar others [21–23], but differs in that the node does not stay in the same state if the sum is equal to 0, rather the node state maps to 0.

RESULTS

Sampling networks

To relate cycling dynamics to the topology of the interaction network, we began by considering random networks. We found that most random networks have a small cycle length (Figure 1.C). Since the tail of the length distribution is exponential and the identification of cycles is NP-hard [24], we can only effectively characterize cycle lengths in small networks. For example, a random network of seven nodes possesses a cycle of length 19 with an approximate probability of one in a million. Edge density is a determining factor in maximal cycle length; denser networks generally express a higher density of networks with long cycles. Furthermore, altering a single edge (e.g., from excitatory to inhibitory) has a destructive impact on the maximal cycle length (Figure 1.D; see also Supplementary Information).

Unlike random networks, biological systems exist under energetic constraints upon interactions or their physical conduits [25, 26]. But the goal of minimizing interactions is countered by the goal of facilitating a diverse dynamical repertoire [27–30]. Accordingly, we stipulated an objective function that arbitrates a trade-off between the maximization of the cycle length and the minimization of network density. Specifically, we used a Pareto algorithm that encodes each network’s genetic representation as a string of n^2 characters in the set $-1, 0, 1$ (see Supplementary Information). Using this genetic algorithm, we evolved random networks along the Pareto front and confirmed that we produced networks with larger maximum cycle lengths than equi-dense random networks (Figure 1.E).

Forbidden motifs

We next turned to examining the networks’ local topology, which differs markedly between evolved and random networks. We sought to identify the mechanism underlying long cycling behavior. We observed that

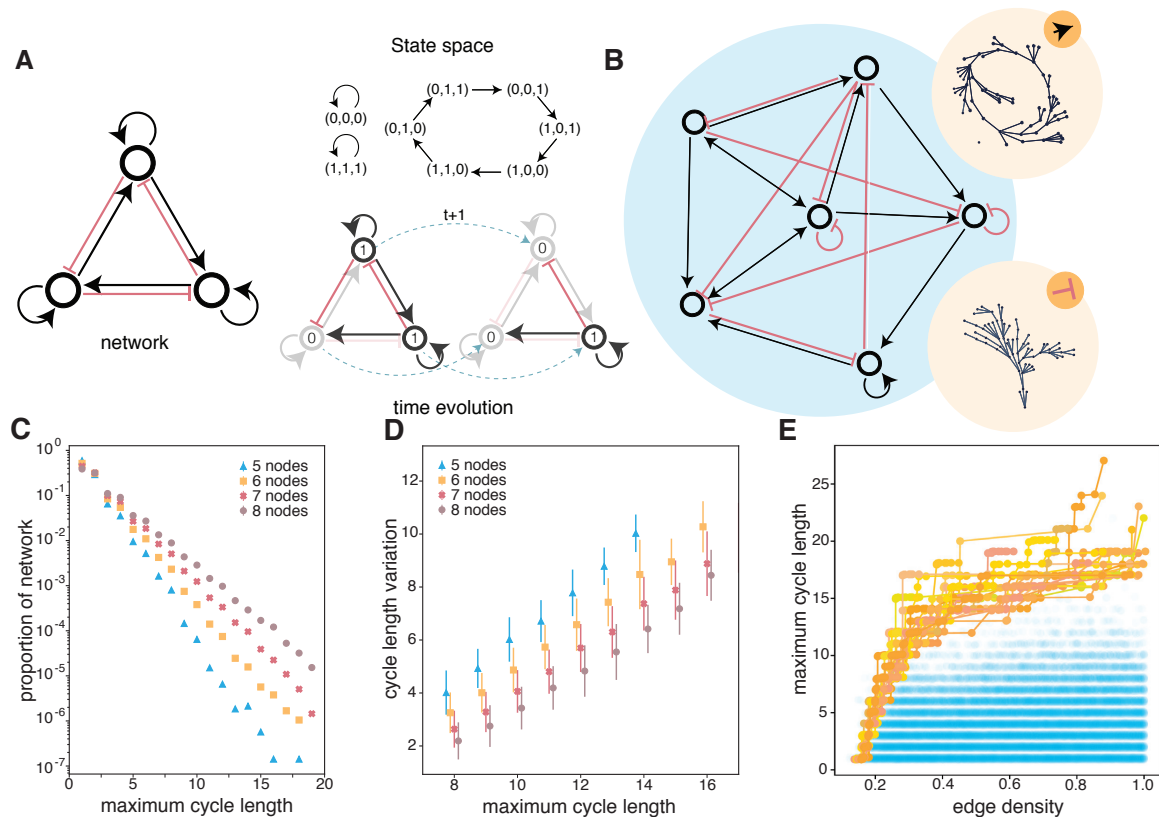


FIG. 1. **Description of the Boolean network model.** (A)(left) A simple example interaction network. Red indicates an inhibitory connection; black indicates an excitatory connection. Curved arrows indicate self-loops. (A)(bottom, right) Two consecutive temporal states of the network on the left. Connections not in use are shown in grey. The state of each node is shown as a ‘0’ or ‘1’ inside the relevant circle. (A)(top, right) The full state space of the network shown on the left. Arrows indicate the temporal progression from state to state. Each state is encoded as the activity of the three nodes (e.g., ‘(0,1,1)’ starting from the top one). (B) A larger interaction network of 6 nodes. The state space of this network will depend upon whether the orange edge is excitatory or inhibitory. In the former case, the state space is as shown in the top beige circle; in the latter case, the state space is as shown in the bottom beige circle. (C) Next, we perform numerical simulations in which we construct networks of size 5, 6, 7, and 8 nodes with different topologies. We first calculate the maximum cycle length (x -axis), and then we determine the expected decrement in cycle length when a single edge is randomly altered (y -axis). The consistently large decrements observed indicate the importance of single edges in cyclic behavior. (D) Optimizing networks for cycle length. The blue data points depict a random sample of networks of different densities. The yellow and orange lines are the Pareto fronts of 25 optimizations where we maximize cycle length and minimize network density. The Pareto optimization algorithm successfully produces networks with unexpectedly long cycle lengths. (E) Networks with large cycle lengths are rare in samples of random networks. We sample from a uniform distribution over the space of all topologies of the interaction network on n nodes (from $n=5$ to $n=8$). Here we show the log-density of networks for a given maximum cycle length and a given number of nodes.

the global properties of the Pareto front networks—specifically, their density and average degree—were similar to those of random networks. Yet, their local topology was dramatically different. When considering the 3-motif, i.e., a subset of three nodes in the graph with their connections, we discovered a subgroup of around thirty (out of a possible 3284) 3-motifs that were almost completely absent in the evolved networks (see Methods and Figure 2.A). These *forbidden motifs* were particularly interesting to study because they suggested a condition on the network’s local connectivity that affected its evolved functionality.

To evaluate the impact of forbidden motifs on cycle

length, we artificially created networks containing a high density of forbidden motifs (see Methods). We found that the average cycle length was significantly lower than expected in random networks, for all network densities ($p < 0.0001$) (Figure 2.B). We also found that the density of networks with a given maximum cycle length was lower than expected in random networks (Figure 2.C). To determine the specificity of the observed behavior, we next constructed networks containing a high density of randomly selected 3-node motifs. In this new population, we did not observe a decrease in the density of networks with a long cycle length (Figure 2.C). These findings suggest that a decremented cycle length is spe-

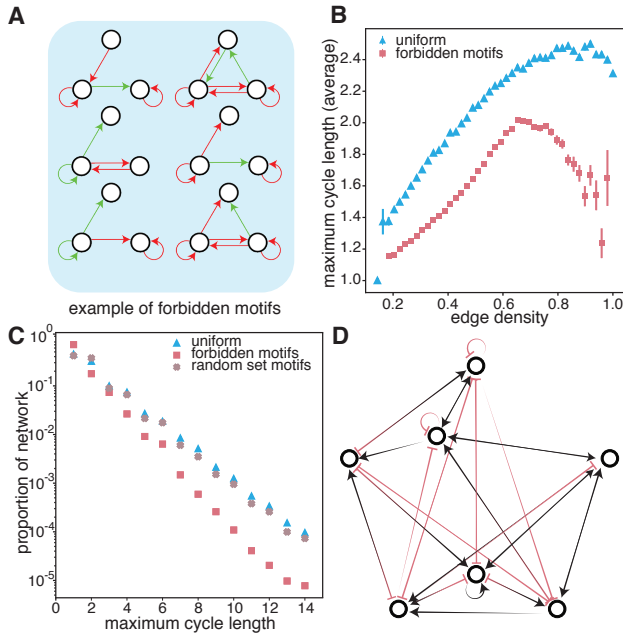


FIG. 2. The role of forbidden motifs in cycle dynamics. (A) A 7-node example of a chimera network with cycle length L and a forbidden motif density of D . Chimera networks have unexpectedly long cycle lengths even if they are mainly composed of motifs known to decrease the cycle length, i.e., forbidden motifs. (B) Average cycle length in randomly sampled networks. The blue data points depict a random sample from a uniform distribution over the space of all interaction network topologies on $n = 7$ nodes. The orange data points represent a random sample over networks created by gluing forbidden motifs together (see Methods). (C) Large cycle lengths are rare in samples of random networks containing forbidden motifs. The red curve represents a random sample over networks created by gluing together a randomly selected subset of all motifs. Here we see that the decrease in cycle length is not caused by the gluing process but by the motifs themselves. (D) Example of forbidden motifs. For the full list, see the Supplementary Information.

cific to forbidden motifs and is not an artifact of a bias towards particular motifs.

However, there is more subtlety to the story than simply the presence of forbidden motifs. Specifically, we found that some networks had both a high density of forbidden motifs and a relatively long maximal cycle length. In what follows, we will refer to these networks as chimera networks. As an example, we found a 7-node network with a maximum cycle length of 21 (see Figure 2.D). More generally, we observed that approximately 1 in 150 million networks that have been constructed to ensure a high density of forbidden motifs had this same maximum cycle length (21), a 98.2% decrease from the expected proportion. Hence, while forbidden motifs generally decrement the network’s dynamical complexity, there is a more fundamental mechanism at play.

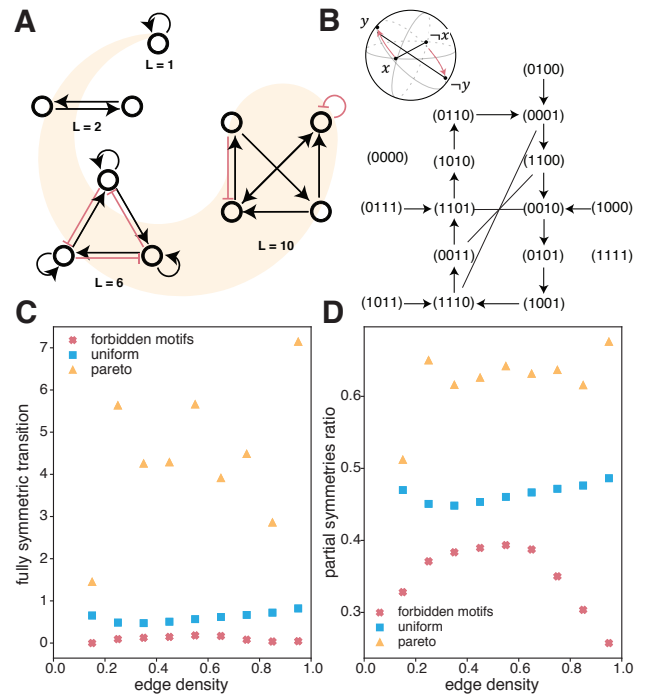


FIG. 3. The role of symmetries in cycle dynamics. (A) Example networks of up to 4 nodes, with the highest cycle length possible in that network size. For $n = 1, 2, 4$, more than one network configuration produces the maximum cycle length; for $n = 3$, only one network does so. Here we display the more symmetrical configuration for each n , and use L to denote the maximal cycle length. (B) The state space of the $n = 4$ network shown in panel (A). The lines without arrow heads represent the states linked under the reflection symmetry (e.g., ‘(0,0,0,1)’ is linked to ‘(1,1,1,0)’). The top right schematic shows conceptually how the reflection symmetry affects the dynamics of the system where a state x is mapped under time evolution to the state y . (C) Networks with a high density of forbidden motifs are less reflection-symmetric than expected, whereas networks from the Pareto evolutionary algorithm are more symmetric than expected. We sample the average partial symmetry ratio for random networks (orange), evolved networks (blue), and forbidden motif networks (red). (D) Reflection symmetry is particularly marked in evolved networks, and meager for the random and forbidden motif networks.

Dynamical reflection symmetry drives long cycles

To better understand what drives the existence of chimera networks and why forbidden motifs exist, we fully enumerated all networks for $n < 5$ (Figure 3.A). For each n , we identified the networks with the maximal cycle length (see Supplementary Information). What do all of these networks have in common? We might naively posit that a symmetry in the structure of the interaction is important, and this explanation seems to hold true for $1 < n < 4$. However, we observed that the 4-node networks with the maximum cycle length were not struc-

turally symmetric, motivating the need for a different explanation.

As an alternative, we considered a dynamical reflection symmetry that manifests in the network's state-space representation. Such a reflection symmetry permits the inverse of a sequence of states as another sequence, and can simply be thought of using the \neg operator, or the standard NOT gate. Under this operator, the state of four Boolean nodes $x = (0110)$ becomes the state $\neg x = 1 - x = (1001)$. Then, when we say *dynamical* reflection symmetry, we mean that if the system's dynamics evolve to map x to y , then the system's dynamics also evolve to map $\neg x$ to $\neg y$ as follows:

$$f(x) = y \iff f(\neg x) = \neg y . \quad (2)$$

We observed dynamical reflection symmetry in the network's state transition diagram in all of the $1 < n < 5$ networks found to have maximal cycle lengths (Figure 3.A-B). This observation motivates the question of whether and how reflection symmetry might relate to forbidden motifs. We found that the maximum cycle length was significantly lower (Figure 3.C) in the forbidden motif networks than in the random networks (pairwise two-sided z -test, $p < 0.0001$; see Supp. Figure 8 for p -values and confidence intervals). In contrast, our evolved networks—built to optimize the maximum cycle length—displayed a 3- to 7-fold increase in reflection symmetric transitions compared to random networks. These findings link reflection symmetry with the presence of forbidden motifs and with the ability of a network to display cyclic behaviors.

To better understand how reflection symmetry might relate to forbidden motifs, we returned to our artificially constructed networks containing a high density of forbidden motifs, and we measured the number of reflection-symmetric transitions. The number of perfectly symmetric transitions is small, and hence it is of value to also estimate partial symmetries. Specifically, we estimate the fraction of bits that respects symmetry (see Supplementary Information). With this broader definition of partial symmetry, we observed a similar trend in which evolved networks showed an increase in the partial symmetry ratio whereas forbidden motif networks showed a decrease (Figure 3.D). These findings motivate further investigations into the causes that might drive correlations between dynamical reflection symmetry, forbidden motifs, and long cycles.

Local excitatory-inhibitory imbalance sufficient for dynamical reflection symmetry

A key question now arises: How is the local topology of the interaction network related to global dynamical properties? Previously, we saw a correlation between a local circuit property (the forbidden motifs) and a global dynamical property (the maximal cycle length) of the system. We can uncover the mechanism by considering

the optimal networks that we previously found for $n \leq 4$ (Figure 3.A). Note that for these networks, the sum of edge weights on each node equals 1; there is always one more incoming excitatory edge (taking the value 1) than incoming inhibitory edge (taking the value -1). In what follows, we will call nodes with this property *well-poised* (Figure 4.A).

This relationship is key to explaining why forbidden motifs are underrepresented in the set of evolved networks. We found that forbidden motifs significantly increased the number of non-symmetric transitions by breaking the well-poised condition (Figure 4.B). To consider the magnitude of the imbalance, we next studied the average squared deviation from being well-poised. We found that the decrease in the balance of the forbidden motif networks was even more discernible via this metric (Figure 4.C). This condition for having symmetry gives a link between forbidden motifs (in the circuit) and reflection symmetric transitions (in the dynamics) (see Supp. Proposition A.9 in Supplementary Information).

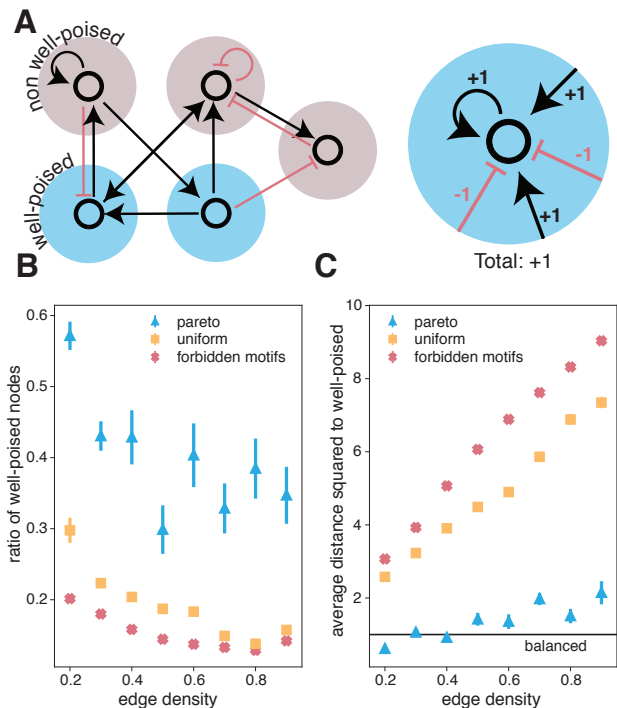


FIG. 4. **Well-poised nodes.** (A) (left) Example of a 5-node network with 3 non well-poised nodes and 2 well-poised nodes. (right) A well-poised node is a node where the total weight of the input is equal to 1. (B) Comparison of the ratio of well-poised nodes in the optimal networks of the Pareto front networks (blue), random networks (orange), and networks with a high density of forbidden motifs (red). (C) Comparison of the average squared distance d between the given nodes and a well-poised node: $d = \frac{1}{n} \sum_i (\delta^+(i) - 1)^2$, where n is the number of nodes and $\delta^+(i)$ is the weighted in-degree of node i given by $\delta^+(i) = \sum_j A_{ji}$. Note that $d = 1$ for a well-poised node.

Similarly, we found that making the nodes' inputs

well-poised coupled with making the nodes' outputs well-poised leads to networks having a time-reversal property. This property implies that no two states are transitioning to the same state and that every state has a state transitioning to them (see Supp. Definition A.2). Finally, we analyzed the impact of local topology on the robustness of our networks to perturbation (see Supp. Section A). We found that the presence of forbidden motifs did not increase their sensitivity compared to random networks (see Supp. Figure 7.B).

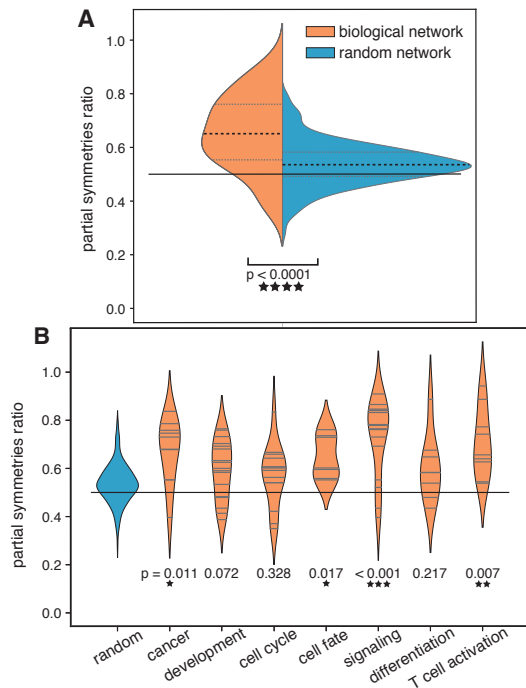


FIG. 5. **Reflection symmetry in gene regulation networks.** (A) Comparison between the average symmetry ratio for Boolean network models of biological systems and their random counterparts built to maintain the joint distribution of node number and nodes' in-degree. (B) Comparison between the average symmetry ratio of Boolean network models of biological systems separated into categories according to tags in the GINim repository.

Biological networks evolved to support reflection symmetries

Evolved networks that displayed a large maximum cycle length tended to express reflection-symmetric transitions more frequently than random networks. Interestingly though, those transitions were not exclusively present inside the cycles but instead were also found in the non-cyclic part of the state space. This observation suggests that dynamical symmetries may play an even deeper role in evolved networks, and motivates investigation of their presence in broader categories of dynamical

networks, both synthetic and natural. To test our hypothesis regarding the presence of reflection symmetries in biology, we turned to gene regulatory networks. We used two repositories: the GINsim software [31] and the PyBoolNet python package [32] (see Supplementary Information).

Using these data, we observed that Boolean models of real biological systems showed markedly more symmetries than random networks (Figure 5.A). Specifically, the average number of symmetric transitions in the biological model networks was 64.4% whereas the average number in random networks was 53.6%. Further, the reflection symmetry ratio was significantly greater in the biological networks than in the random networks (two-sided t -test, $t = 7.068$, $p = 4.6 \times 10^{-10}$). In addition to this overall effect, we noted a marked variation across the different models: for 10 of the biological networks, less than 50% of transitions were symmetric; for 29 of them, more than 70% were symmetric; and for 12 of them, more than 80% were symmetric. To better understand this variability, we divided the models into biologically relevant categories using the tags provided in the GINsim repository. The seven most populated categories were retained for analysis (Figure 5.B). We observed that the most symmetrical categories were cell signaling, cell fate, cell activation, and cancer, with only a few networks lying under the 50% line.

Deriving reflection symmetry directly from data

Boolean networks permit a simple, general definition of dynamical symmetry. However, Boolean models are not available for many natural dynamical systems, and creating them requires extensive work. Hence, here we develop and apply a technique to evaluate reflection symmetry directly from data, circumventing the challenges of Boolean model construction.

We considered the problem of drug resistance in melanoma at the single-cell level. The state of gene expression can predict which cells will be resistant to therapy and which ones will be sensitive and responsive to therapy. Notably, this prediction is possible before the cells have been treated with any drug. Thus, we define the state of a cell as a “primed” resistant state if that cell would be resistant upon the application of a drug [33]. For this experiment, we profiled the gene expression of these cells using scRNA-seq. We then divided the cells into two categories: the drug-sensitive cells and the cells primed for drug resistance [33].

To apply the idea of symmetry to these data, we normalized the expression of each gene. Specifically, negative (positive) normalized quantities represented a lower (higher) level of expression than the average expression found for a given gene in all the cells tested. We then defined a parity metric to determine whether two cells had a symmetric expression at the gene level. This metric quantifies how opposite the expressions of the same gene

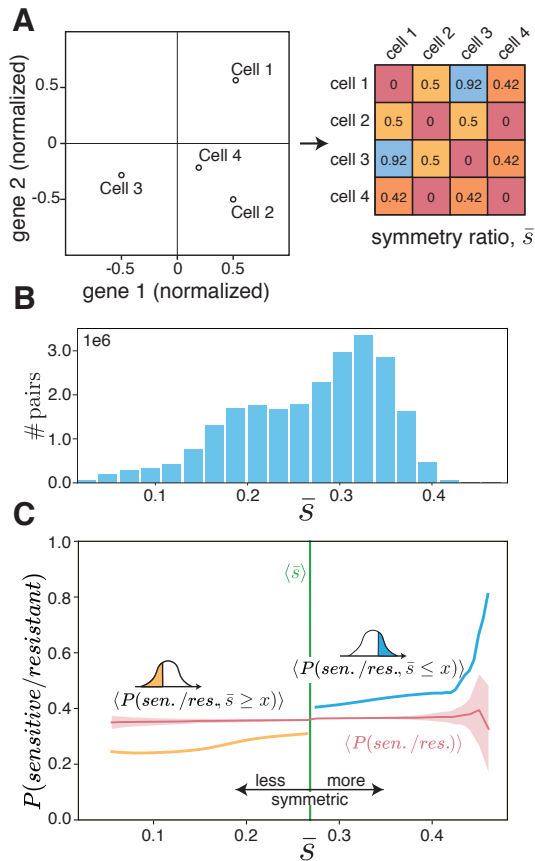


FIG. 6. Reflection symmetry in cancerous cells. (A) An example of the reflection symmetry ratio for four cells that express two genes. (Left) The normalized level of expression for all four cells and both genes. (Right) A symmetric matrix showing the computed reflection symmetry ratio between every pair of cells. In this example, cells 1 and 3 are highly reflection-symmetric whereas cells 2 and 4 are not reflection-symmetric (asymmetric). (B) The probability for a randomly selected pair of cells to have different states (drug sensitive state/drug resistant state) as a function of the reflection symmetry ratio \bar{s} under different conditions. The orange curve shows the probability for pair of cells that were less symmetric than the average reflection symmetry ratio (green line) for a given maximal symmetry as marked by the x -axis. Their probability is lower than the average probability obtained by random permutations of the labels (red line). The blue curve shows the probability for more reflection-symmetric pairs than the average for a given minimal symmetry as marked by the x -axis. (C) The distribution of the reflection symmetry ratio (\bar{s}) for all pair of cells.

are for two different cells. The metric is equal to 1 for perfect symmetry and 0 for a complete lack of symmetry (see Figure 6.A and the Supplementary Information). We observed that the distribution of the parity metric spanned from 0 (non-symmetric pairs) to 0.4 (symmetric pairs). The distribution was also bi-modal, suggesting the existence of two pair types (see Figure 6.B).

With these data and metrics in hand, we studied the

effect of reflection symmetry by taking the known states (drug-sensitive or primed for resistance) as symmetric paths. Specifically, we computed the probability that a pair of cells respecting a given criterion were of different states (drug-sensitive or primed). When considering all pairs independently from their reflection symmetry, we observed a probability of around 35% for a pair to have different states. We expected pairs with a high (low) reflection symmetry ratio to have a higher (lower) probability of residing in different paths (drug-sensitive vs. primed). Our expectation was confirmed: pairs with a low reflection symmetry ratio had a probability of around 25% to be of different states versus 80% for the high reflection symmetry ratio pairs (see Figure 6.C). Broadly, these data demonstrate that reflection symmetry is predictive of drug resistance in cancer.

DISCUSSION

Functional Role for Reflection Symmetry.

In this study, we uncovered a new link between the expression of specific motifs and the existence of cycling behavior in Boolean networks. Potential links between these two properties have been reported previously for some gene regulatory networks [34]. For example, prior studies report a link between bi-fan motifs and cycling behavior [34], and find that chaotic motifs are linked to cycling [35]. However, the relationship presented in our study is of a novel type, formally linking abnormally underrepresented motifs and their function as reflection-symmetry breakers. This relationship gives a clear explanation for how an interaction network with these motifs has the ability to maintain long cycles. Our mechanistic approach allows us to more rigorously interpret the data in prior studies, which has until now remained correlative in nature.

Diversity of Dynamical Symmetries.

Although here we have investigated the problem of dynamical symmetries in Boolean networks, many other types of symmetries exist. For example, one might seek to understand symmetries in the output function on each node, and consider that the function $f_1(\vec{x}) = x_1$ or x_2 is invariant under permutation of its argument. In fact, output function symmetries at the node level are a powerful way to characterize complex network dynamics [36, 37]. Our work extends these observations by showing that symmetries on the global level can elucidate networks with complex dynamics. Another common approach is the study of symmetric properties inside the interaction network, such as fibration symmetry [38, 39]. Our approach differs from these studies in evaluating symmetry in the state space [40], but nevertheless

provides insights regarding a specific property of the interaction network. This property does not appear as a symmetry in the structure, but as a balancing equation on each node. By taking a different perspective from prior studies, our approach sheds light on new mechanisms of dynamical symmetries and the function of the systems that support them.

Methodological Considerations.

Several methodological considerations are pertinent to our work. First, there remains a conceptual and formal distinction between a system and its Boolean network model. Here we have shown that biologically inspired Boolean networks display a high level of dynamical symmetry and that not all biological processes have the same amount of symmetry. Yet, it remains unknown whether reflection symmetry is intrinsic to the system or a result of the map between a set of experiments and its Boolean network model. Hence, future work could examine the impact of the mapping process on our reported findings. Further experimental work could examine the evolution of a simple biological system (e.g., yeast) and confirm the existence of reflection-symmetric states.

The typical approach of modeling biological systems uses a general form of the model which includes more general types of Boolean interaction. However, we note that reflection symmetry can be easily identified in both thresholded and unthresholded models. Since every Boolean model maps binary states to binary states, our reflection symmetry definition is broadly applicable and is not dependant on the nature of the updating scheme. The difference in model only affects our ability to analyze possible motifs, since the model determines the type of interactions.

The application of symmetry analysis to gene expression inside melanoma scRNA-seq data is a simple example of data classification done using symmetry. However, the drug-sensitive and drug-resistant paths were not directly observed in the cells where the gene expression was measured. The labeling was inferred by principal component analysis of the cells' gene expression, where the variance was found to be principally located on one axis. This axis was later found to correlate highly with sensitivity and drug resistance. Additional studies should be conducted on data sets that are not linearly separable using one axis and on data expressing more than a binary category.

Finally, our theoretical results hold for a simple type of Boolean model that is less general than the one used in many biological networks. Future work could seek to generalize and test the theory of dynamical reflection symmetry for general Boolean networks. Further work could test and apply the theory to random Boolean networks, a model often studied by physicists in a similar contexts [18, 41].

FUTURE DIRECTIONS

Our results can be used to improve the power of Boolean network modeling of real systems. By searching for network representations in the symmetric subspace of all possible networks for a given data set, finding Boolean network models could necessitate less data while being faster. This is important for the practical use of Boolean modeling since it is, in practice, impossible to explore the complete state space using expensive experiments. Another way to use the reflection symmetry in generating new Boolean models of real phenomena is to include the reflection-symmetric counterpart to the experimentally observed trajectories in the training data set. This approach is, in essence, equivalent to mirroring images used for training convolutions neural networks, which almost double the information contained in the data set at no experimental cost.

As shown, perturbation propagation acts quite differently in the Pareto population than in the forbidden motifs population. Perturbations are on the brink of propagating in the former but not the latter. This effect hints at a potential link between symmetry and criticality, where forbidden motifs drive the system away from critical dynamics. Further experiments on a large ensemble of random Boolean networks are needed to verify this putative link.

Additional studies are also needed to further probe the concept of dynamical reflection symmetry for biological systems. Examples of essential questions include: What causes and regulates dynamical symmetries? Why does the degree of dynamical symmetry vary across different cellular and molecular processes? Which diseases or other perturbations to the system impact this symmetry? Is the symmetry explained by evolution or caused by the physics of the system? Answering any one of these questions has the potential to substantially impact our fundamental understanding of biology.

CONCLUSION

Here we demonstrated that reflection symmetry is significantly over-expressed in Boolean models relevant to many areas of biology. We observed this symmetry while studying the cycling properties of optimal Boolean networks and related it to the under-expression of certain motifs. These forbidden motifs affected the network's cycling ability and negatively impacted the number of reflection-symmetric state transitions. We offered a formal proof relating dynamical reflection symmetries to excitation-inhibition balance in the interaction network, and further explained the relationship between reflection symmetry and time reversal. Our study lays the groundwork for future efforts to determine the cause of this symmetry in general Boolean models and to understand the functional role of this symmetry in biological systems.

ACKNOWLEDGMENTS

M.O. acknowledges support of the support of the Natural Sciences and Engineering Research Council of Canada (NSERC). J.Z.K. acknowledges support from the NIH T32-EB020087. D.S.B. acknowledges support from the National Science Foundation (IIS-1926757, DMR-1420530), the Paul G. Allen Family Foundation, and the Army Research Office (W911NF-16-1-0474, W011MF-191-244). The content is solely the responsibility of the authors and does not necessarily represent the official views of any of the funding agencies.

CITATION DIVERSITY STATEMENT

Recent work in several fields of science—including physics and biology, where our work here is situated [42–46]—has identified a bias in citation practices such that papers from women and other minority scholars are under-cited relative to the number of such papers in the field [47–51]. Here we sought to proactively consider choosing references that reflect the diversity of the field in thought, form of contribution, gender, race, ethnicity, and other factors. First, we obtained the predicted gender of the first and last author of each reference by using databases that store the probability of a first name being carried by a woman [44, 52]. By this measure (and excluding self-citations to the first and last authors of our current paper), our references contain 5.64% woman(first)/woman(last), 13.33% man/woman, 11.4% woman/man, and 69.64% man/man. This method is limited in that a) names, pronouns, and social media profiles used to construct the databases may not, in every case, be indicative of gender identity and b) it cannot account for intersex, non-binary, or transgender people. Second, we obtained predicted racial/ethnic category of the first and last author of each reference by databases that store the probability of a first and last name being carried by an author of color [53]. By this measure (and excluding self-citations), our references contain 29.6% author of color (first)/author of color(last), 11.7% white author/author of color, 16.78% author of color/white author, and 41.93% white author/white author. This method is limited in that a) names and Florida Voter Data to make the predictions may not be indicative of racial/ethnic identity, and b) it cannot account for Indigenous and mixed-race authors, or those who may face differential biases due to the ambiguous racialization or ethnicization of their names. We look forward to future work that could help us to better understand how to support equitable practices in science.

METHODS

Evolutionary algorithm

In our evolutionary algorithm, we set the population size to 600 interaction networks with a density taken from a uniform distribution ranging from 0.2 to 1.0. The selection for mating is handled by the NSGA2 algorithm [54]. In each step, 400 new offspring are created using two mating operators (see next section for details). We mutate each edge of the offspring’s interaction networks with a probability of $P = 0.02$. When a component is selected for mutation, its value is changed to one of the two other values in $\{-1, 0, 1\}$. The generation process is repeated 300 times, a number which is chosen to be significantly greater than the convergence time. The whole process is repeated 30 times.

Mating operators

We use two mating operators that reflect the exploratory and convergent mating strategies, respectively. Both operators are used with equal probability each time we call the mating procedure. The first mating operator generates two offspring. For each index of the matrix, each offspring gets assigned either the first or second parent’s component. If the first offspring receives its component from parent two, then the second offspring receives its component from parent one. Then both matrices are tested for validity; if one is found to be disconnected when considering the interaction matrix as an undirected graph, the process is restarted. The second mating operator generates one offspring at a time. We list the cycle basis of both parents’ interaction networks. Then, random cycle structures are picked from the cycle basis to build a new interaction network containing a random mixture of cycles from both parents. Only cycles that agree for all of their common inhibition or excitation edges are selected. If two selected cycles cannot be joined together because of disagreeing edges, then the process is restarted. If the process fails more than 1000 times, we use the first mating operator. Such failures happen but are rare and represent a negligible percentage of the offspring production.

Sampling

For the unbiased case, we sample in two steps. First, a density is chosen uniformly at random from the range 0.2 to 1. Second, we select elements in the matrix and fill those elements with either a -1 or $+1$ —with equal probability—until we reach the target density. For the biased case, we again begin by choosing a density uniformly at random from the range 0.2 to 1. Then, we select valid motifs at random from the set of desired motifs and place them randomly in the interaction network.

If we cannot find a position for a given motif, then we discard that motif and randomly draw another from the same set. Once the desired ratio of motifs is achieved, the network is filled with random edges to achieve the global density. Edges used for a motif (empty edges included) are protected and cannot be filled in this part of the process.

Motif characterization

To calculate the z -value for the number of expected motifs, we used sampled data to obtain the average expected number of each motif and the standard deviation of the expected number. Since the expected number for 3-motifs is always one order of magnitude less than the standard deviation, we consider motifs with an individual z -score of less than -0.1 to be repressed. This repression typically corresponds to the absence of the motif in the graph. We then consider a given motif to be repressed in the population if it is tagged as repressed in at least 50% of the population's individual graphs.

Reflection symmetry in real cells

We first clean the list of analyzed genes to accelerate the data processing and to simplify the definition of reflection symmetry. Genes that are highly expressed in more than 70% of the cell are removed as these are typically housekeeping genes unrelated to the process of interest. We also remove genes that are not expressed in at least 25% of the cells since it becomes too hard to find two cells having the same gene expressed. Genes with zero expression are changed to NaN. Finally, genes with a decreasing expression distribution, i.e. where most expression values are close to 0, are removed because of their lack of suitability for defining a symmetry axis.

For each gene, the maximum of the distribution of each gene's expression over all cells is defined as the zero expression level. Redefining the zero expression allows us to think of the expression of each gene as being more (positive value) or less (negative value) than the most common quantity found in the cells. The maximum of the distribution was preferred over the average since the distributions have highly zero-inflated counts due to the experimental technique used. The expression value for each gene is then scaled by the standard deviation. Let x be a gene, i, j be a pair of cells, and $s(i, j)$ be the reflection symmetry ratio. We ask for the function $s(i, j)$ to be 1 for perfectly symmetric expression, i.e. $x_i = -x_j$. We also desire that the function will output a 0 if $|x_i| \approx 0$ and $|x_j| \approx 0$ even if $x_i = -x_j$. This condition allows us to avoid attributing some symmetry properties to noise by requiring a difference of at least 20% of the standard deviation between the two expressions x_i and x_j . Finally we want the function to output a 0 when x_i and x_j are of the same sign. One possible function with these

properties is given by

$$s(i, j) = 1 - \max \left\{ \left| \frac{x_i + x_j}{|x_i| + |x_j| + \epsilon} \right|^{h_1}, \frac{1 - \tanh h_2 (r_{x,ij} - r)}{2} \right\},$$

where h_1, h_2 are parameters that select the smoothness of the transition between the values of 0 and 1, and $r_{x,ij} = \sqrt{x_i^2 + x_j^2}$. The parameters used for the indicator are $h_1 = 1.7$, $r = 0.1$, $h_2 = 25$, and $\epsilon = 1 \times 10^{-7}$.

Appendix A: Appendixes

SUPPLEMENTARY INFORMATION

The model

The apparent simplicity of this Boolean model belies surprising complexity. Unlike Hopfield networks, the lack of symmetry in the interaction matrix ($a_{ij} \neq a_{ji}$) of Boolean networks implies the non-existence of a Lyapunov function, making them difficult to study analytically [55, 56]. Further, the inclusion of self-loops has been shown to increase the number and robustness of attractor states, thereby increasing the complexity of our model’s dynamics [57]. For these reasons, such models are remarkably expressive and useful in explaining real biological observations such as cell differentiation [58].

To determine correlates of cycle length, we studied the relationship between a network’s maximum cycle length and the density of inhibitory versus excitatory edges (see Supp. Fig. 11B). Further, we found that the average maximum cycle length increases with the presence of excitatory or inhibitory circuits in the interaction network (see Supp. Fig. 11C). We also found that the specific distribution of excitatory and inhibitory connections, particularly in self-connections, differentially affected cycle length. Self-inhibition, which we defined as an inhibition circuit of length 1, was positively correlated with a high maximum cycle length. By contrast, self-excitation, which we defined as an excitatory circuit of length 1, was negatively correlated with a high maximum cycle length (see Supp. Fig. 11D).

Evolved networks

Each node in the evolved networks had approximately 20% more incoming excitatory edges than inhibitory edges. The evolved networks also exhibited nearly twice as many physical excitation circuits as the random networks (see Supp. Fig. 9D). These features were emergent properties, as the evolutionary algorithm did not explicitly optimize for them. In addition to comparing all evolved networks to all random networks, we separately examined the dynamics of evolved networks that implemented the exploratory versus the convergent mating strategy. We found that convergent mating consistently produced networks with greater maximum cycle length than exploratory mating (see Suppl. Fig. 9C).

Reflection symmetry

Since for each $n \leq 4$ there was at least one network with the maximal possible cycle length with this symmetry, it is quite tempting to conjecture that there always exists a maximal network with this property. This, of

course, cannot be confirmed computationally and could only be realistically verified up to $n = 5$ without developing a more sophisticated search algorithm. The symmetry forces the $\vec{1}$ state to map to itself since the $\vec{0}$ state always maps to itself. It is also possible to prove that there is no n such that a cycle of length $2^n - 1$ will be possible other than for $n = 1$ (see Proposition A.5).

We prove that the condition on the excitatory-inhibitory balance is sufficient to produce reflection-symmetric transitions in the state dynamics (see Proposition A.9). Further, this condition is not only sufficient, but is *equivalent* to reflection symmetry. Therefore, the existence of reflection symmetry in state dynamics implies that the number of incoming excitatory edges is one more than the number of incoming inhibitory edges on all nodes in the interaction network. In this way, the condition relates the system’s global dynamics to the local properties of the interaction network.

Robustness

Another frequently cited property of the evolved networks is their robustness to perturbation. We sought to determine if the evolved networks and the forbidden motif networks had distinct levels of robustness. The notion of robustness depends upon a notion of response to perturbation. The distance between the non-perturbed and perturbed states is measured at each time step by the Hamming distance, which only counts the number of non-matching bits. A robust network is one where the distance stays constant or decreases over time. We expect evolved networks to show an increase in robustness, and we expect forbidden motif networks to show a decrease in robustness. The results are surprising: for a large range of edge densities, perturbations to forbidden motif networks do not drive a large divergence in state dynamics in comparison to uniform random networks (Supp. Fig. 7). In contrast, evolved networks are significantly less robust to perturbations.

Intuitively, one might imagine that a network’s sensitivity to perturbation could depend upon the maximum cycle length, such that the longer the maximum cycle the greater the tendency for perturbations to drive divergent dynamics. In contrast to this intuition, however, random and forbidden motif networks have quite different average cycle lengths. The difference could then be entirely caused by the presence of long cycles in the evolved population in comparison with the two other populations. To test this possibility, we have compared networks from each category with the same cycle length. For a given maximum cycle length, evolved networks have a slightly lower distance than the random and the forbidden networks for a given cycle length (see Supp. Figure 10.A). The difference however is quite small and is cyclic with the period equal to the cycle length, as expected (see Supp. Figure 10.B). Therefore, forbidden motifs and the optimization process have, for a given maximum cycle

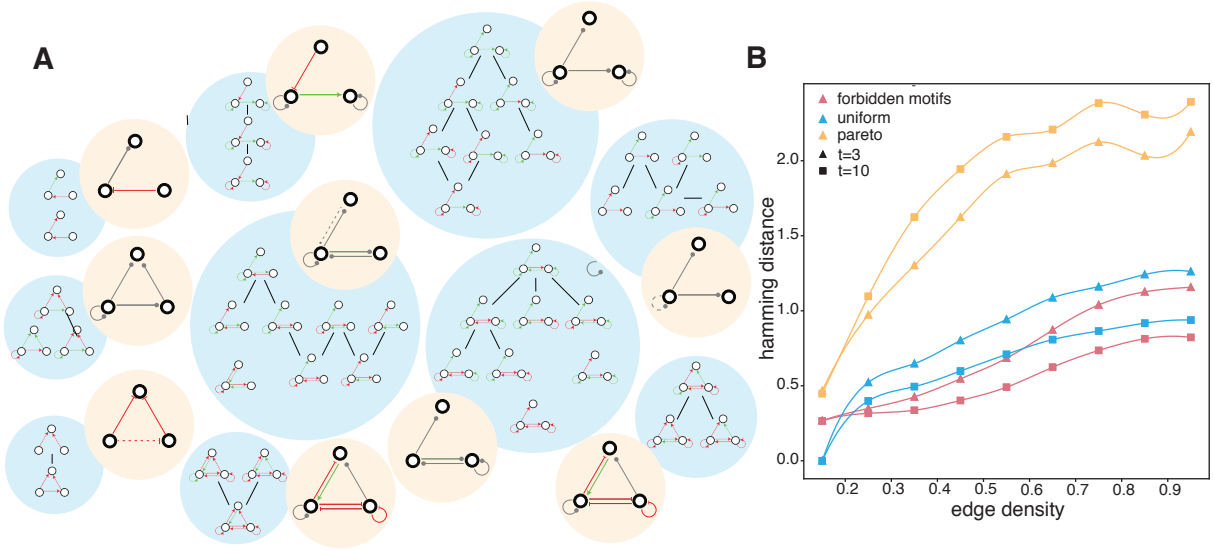


FIG. 7. **Forbidden motifs and their impact on the propagation of perturbations.** (A) To improve the readability of this visualization, the set of forbidden motifs was approximately clustered by structural similarity. Each blue circle represents a cluster. The line between motifs inside a cluster shows how motifs in the cluster are related. The beige circle represents the global structure of the motifs inside the blue cluster. (B) Small perturbations propagate more in evolved networks than in random and forbidden motif networks. We sample the average distance between two states which initially differs only by one component after 3 updates (triangle) and after 10 updates (square).

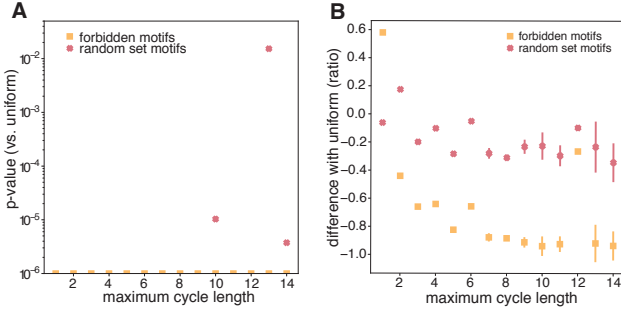


FIG. 8. **Statistical analysis.** (A) The p -values for the comparison with the uniformly sampled networks shown in Figure 3.D. The p -values were capped at 10^{-6} when their values were smaller than this number. (B) The ratio of difference with the uniformly sampled networks showing the confidence interval as error bars.

length, a rather low impact on how the networks handle perturbations.

Time reversal

After a number of transitions longer than the longest transient chain of states, the system is necessarily stuck in a cycle (possibly of length 1). In that case, it is possible to infer the previous state visited by the system from the current state of the system; and similarly, it is possible to construct a system that would traverse the cycle in the opposite direction, as if we had reversed the arrow of

time. For some networks, only the states in the cycle can be reversed, whereas for other networks all of the states in the entire system can be reversed. The latter property is called *bijection*, and implies that no two states are transitioning to the same state and that every state has a state transitioning to it.

Several interesting properties arise when considering *bijection*. In this model, reflection symmetry is a necessary condition for the transition function to be *bijection* (see Proposition A.10). Therefore, all *bijection* networks are reflection symmetric. However, not all reflection-symmetric networks are *bijection*. When considering the operation of reversing the interaction direction in a network (transpose of A), we find that all *bijection* networks tested always transform to another *bijection* network. Put differently, for all *bijection* networks tested, reversing the interaction direction always produces the inverse time evolution. Therefore, the transpose of A seems to act on the subset of *bijection* networks as a time-reversal operator. Finally, the optimal networks up to $n = 3$ are *bijection* but those for $n = 4$ are not. Therefore it is not a necessary condition for being an optimal network.

For the reflection-symmetric case, we proved that the property was equivalent to having a matrix with row sums equal to 1. We can find a similar statement for the time-reversal symmetric case. This symmetry seems equivalent to having a row sum of 1 (at least for $n \leq 4$), thus implying reflection symmetry with the added condition that the column sum is also 1. In fact, these two statements are equivalent for $n \leq 4$. When the input is well-posed, the network displays reflection symme-

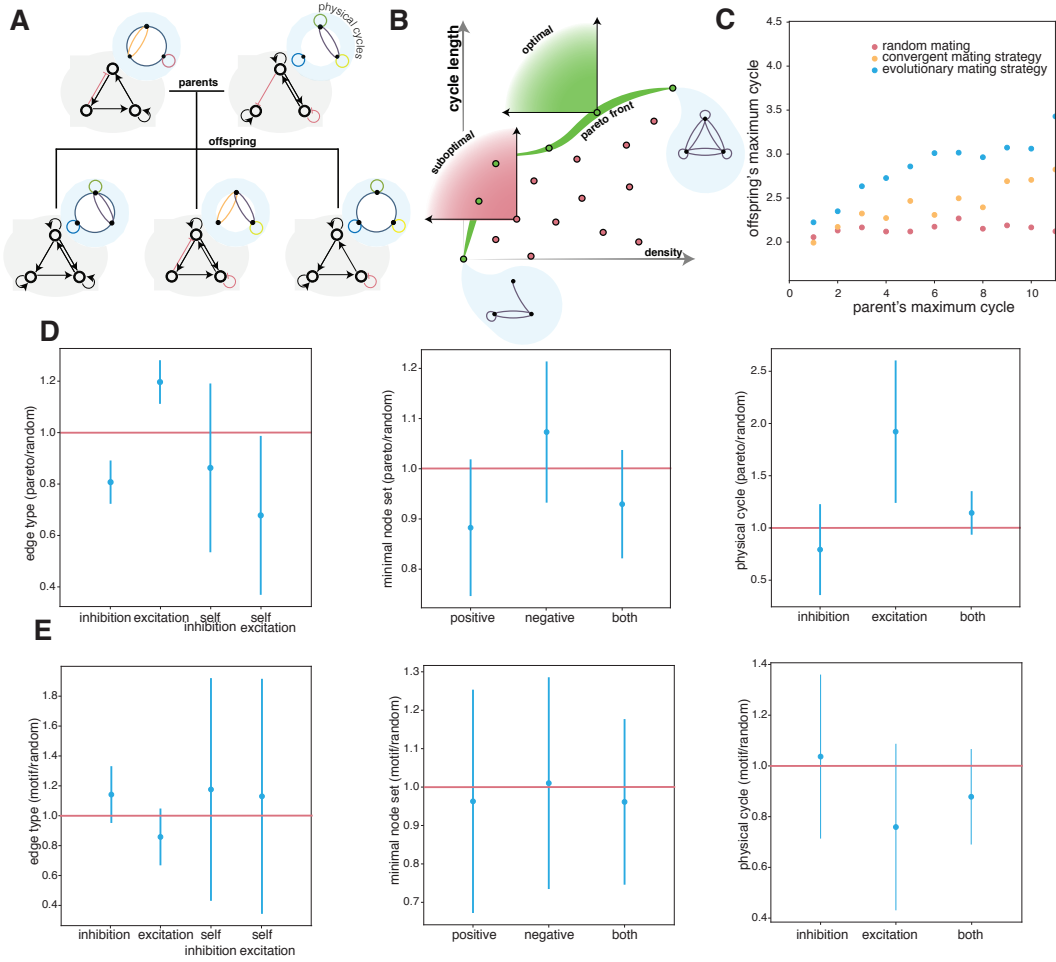


FIG. 9. **Offspring generation and properties of forbidden motifs.** (A) Offspring generation is based on cycle preservation. (B) Example of the approximated Pareto front where green points are optimal in the Pareto sense, and where red points are sub-optimal. (C) Evaluation of the different mating strategies or policies that generate offspring. (D) Ratio of the number of different physical constituents of the Pareto front networks versus random networks. (E) Ratio of the number of different physical constituents for the forbidden motif networks versus the random networks.

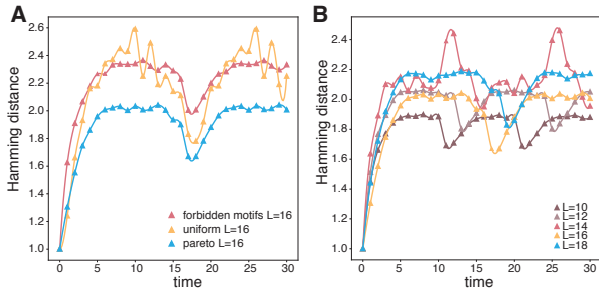


FIG. 10. **Time evolution of perturbations.** (A) Average Hamming distance from the 1-bit perturbed network to the unperturbed network as a function of the time for the Pareto front's networks binned by cycle length. (B) Same as in panel (A) but for a maximal cycle length of 16 and plotted separately for Pareto front networks, random networks, and forbidden motif networks.

try; when both the output and input are well-poised, the network displays reflection symmetry *and* time reversal. The latter conjecture would imply that time reversal forces each node to send a peculiar balance of information to their surroundings with only one more positive edge than the number of negative edges. Collectively, these observations regarding time reversal underscore the fact that again global properties can be explained in terms of local ones in the interaction network.

MATHEMATICAL PROOF

This section will give proofs for several properties presented in the main text. To do so, we will need to develop some tools and nomenclature. Let n be the number of nodes in our Boolean model. To represent each step of the Boolean network in equation 1 we will work primarily

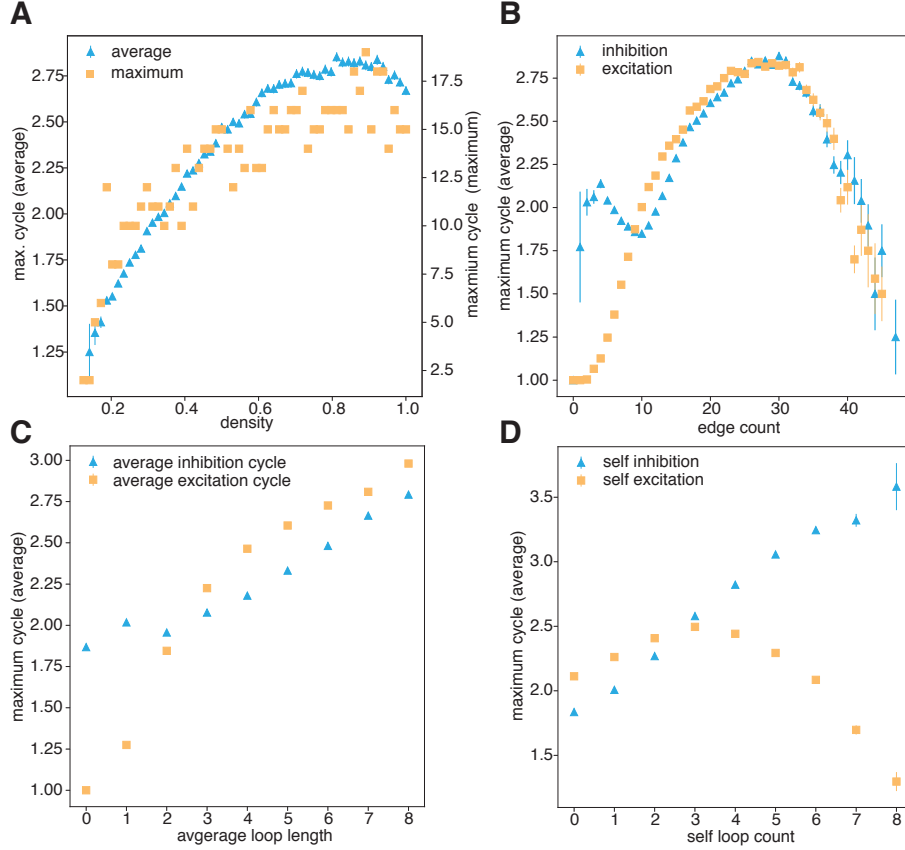


FIG. 11. **Topological properties of random networks.** (A) The average and largest maximal cycle length as a function of density for an eight-node network. (B) The average maximal cycle length as a function of the number of edges of each type: excitatory and inhibitory. (C) The average maximal cycle length as a function of the average size of physical cycles within the interaction network. Note that the former is a dynamical property and the latter is an interaction property. (D) The average maximal cycle length as a function of the number of self-loops, as given by the diagonal entries in the adjacency matrix. All plots use a sample of 400,000 random networks.

with three spaces.

First, we denote \mathbb{Z}^n as the space containing all n -dimensional vectors of integers where the sum $\sum_j A_{ji}x_j(t)$ of equation 1 lies. Second, we denote $\mathbb{B}^n = \{\text{True}, \text{False}\}^n$ as the space containing the Boolean states, which we later convert to integers by mapping True to 1 and False to 0, thereby forming the state vector $x(t)$. Multiple useful binary and unary operators act on this space such as \neg, \vee, \wedge , the negation, the OR-gate, and the AND-gate, respectively. To determine if the component $x_i(t+1)$ is 0 or 1, we only need to know the sign of the right-hand side of equation 1. All components greater than 0 are mapped to 1, and the rest are mapped to 0.

For this purpose, it is helpful to define a third set $S = \{+, -, \star\}$ which represents the knowledge that we have of the sign of the result of an operation. The element $+$ $\in S$ is used to express a positive value greater than zero, and the element $-$ $\in S$ is used to express a negative value or 0. We use $\star \in S$ to describe an unknown sign that can arise, for example, when adding a negative number and a positive number together, the final result of which is

thereby an unknown sign. We will let $S^n = \{+, -, \star\}^n$ be the set of the Cartesian products of n elements from the set S . On this set, we define the binary operation \oplus which recreates the knowledge that we have of the sign of the sum of an addition given the signs of the summands. The operator \oplus acts element-wise according to the following table:

\oplus	+	-	\star
+	+	\star	\star
-	\star	-	\star
\star	\star	\star	\star

As an example, we have that $(+, -, \star, +) \oplus (-, -, +, +) = (\star, -, \star, +)$. A similar operator can be defined for subtraction and multiplication with different tables. We will then define maps that allow us to pass from one set to another (Figure 12).

We also need some machinery to be able to move between the spaces \mathbb{Z}^n, S^n and \mathbb{B}^n . They are listed below:

ι : This map sends an element from the space \mathbb{B}^n to

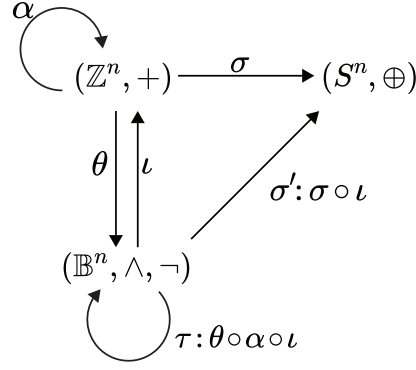


FIG. 12. **Main sets and operations defined on them that are used in the proof.** The different maps used between those sets are also represented.

the space \mathbb{Z}^n , representing the common convention of Boolean algebra where True is mapped to 1 and False to 0 element-wise. Therefore $\iota : \mathbb{B}^n \rightarrow \mathbb{Z}^n$ where for $\vec{b} \in \mathbb{B}^n$ we have

$$\iota(\vec{b})_i = \begin{cases} 1 & b_i = \text{True} \\ 0 & \text{otherwise.} \end{cases}$$

θ : This map is the threshold function that sends elements from the space of integers \mathbb{Z}^n to the space of Boolean values \mathbb{B}^n where $\theta : \mathbb{Z}^n \rightarrow \mathbb{B}^n$ where for $\vec{x} \in \mathbb{Z}^n$. We have

$$\theta(\vec{x})_i = \begin{cases} \text{True} & x_i > 0 \\ \text{False} & \text{otherwise.} \end{cases}$$

σ : This map sends elements from the space \mathbb{Z}^n to S^n using the literal meaning of what the elements of S represent. Therefore, $\sigma : \mathbb{Z}^n \rightarrow S^n$ where for $x \in \mathbb{Z}^n$ we have

$$\sigma(\vec{x})_i = \begin{cases} + & x_i > 0 \\ - & \text{otherwise.} \end{cases}$$

In this case, because we know the sign of the element, \star is not in the image of σ . This map can be used to define a map $\sigma' : \mathbb{B}^n \rightarrow S^n$ such that $\sigma' = \sigma \circ \iota$. This map sends True to + and False to -. Often, we will often denote this map by σ when it is clear from the context.

Using these three simple maps, we can define an endomorphism from these spaces to themselves, reproducing the system's dynamics. They are presented below:

α : This map is simply the one generated by the product of the rule matrix A of a given network such that $\alpha : \mathbb{Z}^n \rightarrow \mathbb{Z}^n$ where $x \mapsto A^\top x$

τ : We call this map the transition function. It updates the Boolean network sending each state in \mathbb{B}^n to the next state in \mathbb{B}^n following equation 1 such that,

$$\tau(b) = \theta(\alpha(\iota(b))). \quad (\text{A1})$$

An important property of the set of signs S^n is that it is invariant under the projection of the threshold map θ such that

$$\sigma(\iota(\theta(x))) = \sigma'(\theta(x)) = \sigma(x) \quad x \in \mathbb{Z}^n. \quad (\text{A2})$$

A simple but essential relation in the space of binary vectors is a binary relation called the valid pair relation, given by the symbol \sim . Two binary vectors in \mathbb{B}^n are a valid pair if they do not share any True elements, or more precisely if,

$$a \sim b \iff a \wedge b = \text{False}^n, \quad a, b \in \mathbb{B}^n \quad (\text{A3})$$

where False^n is the n dimensional vector of False in \mathbb{B}^n . Valid pairs have useful properties. A simple and useful property is that for $a, b \in \mathbb{Z}^n$ we have that,

$$a \sim b \implies \iota(a \vee b) = \iota(a) + \iota(b). \quad (\text{A4})$$

The following proposition demonstrates that for a Boolean vector comprising the union of a valid pair, $c = a \vee b$, the sign of the transition of the vector, $\tau(c)$, is related to the sign of the transitions of its composite valid pair, $\tau(a)$ and $\tau(b)$. This relation is our primary tool to tackle the problems at hand.

Proposition A.1. For $a, b, c \in \mathbb{B}^n$ such that $a \sim b$ and $a \vee b = c$, we have that

$$\sigma'(\tau(a)) \oplus \sigma'(\tau(b)) \approx \sigma'(\tau(c)), \quad (\text{A5})$$

where \approx is a symmetric, reflexive, and non-transitive binary relation taken element-wise on \mathbb{B}^n defined by $\{- \approx \star, + \approx \star\}$ and their reflexive counterparts.

Proof. The proof is rather straightforward and is ob-

tained by :

$$\begin{aligned}
\sigma'(\tau(c)) &= \sigma'(\theta(\alpha(\iota(c)))) && \text{A1} \\
\sigma'(\tau(c)) &= \sigma'(\theta(\alpha(\iota(a \vee b)))) && a \vee b = c \\
&= \sigma'(\theta(\alpha(\iota(a) + \iota(b)))) && \text{A4} \\
&= \sigma'(\theta(\alpha(\iota(a)) + \alpha(\iota(b)))) && \alpha \text{ is linear} \\
&= \sigma(\alpha(\iota(a)) + \alpha(\iota(b))) && \text{A2} \\
&\approx \sigma(\alpha(\iota(a))) \oplus \sigma(\alpha(\iota(b))) && \text{def. } \oplus \\
&\approx \sigma'(\theta(\alpha(\iota(a)))) \oplus \sigma'(\theta(\alpha(\iota(b)))) && \text{A2} \\
&\approx \sigma'(\tau(a)) \oplus \sigma'(\tau(b)) && \text{A1}
\end{aligned}$$

□

An important property of transition functions that will be used in the following proofs is bijectivity.

Definition A.2. Let $B \subset \mathbb{B}^n$ and let

$$\tau^{-1}(B) = \{a \mid \tau(a) = b, b \in B, a \in \mathbb{B}^n\},$$

be the set of elements of \mathbb{B}^n that maps to elements of B . Then a bijective transition function is a function such that

$$\text{card}(\tau^{-1}(B)) = 1, \quad \forall b \in \mathbb{B}^n.$$

The discreteness and finitude of the state space imply that bijectivity is equivalent to surjectivity or injectivity. The transition function's surjectivity implies that the system can reach every state in \mathbb{B}^n . This is not always the case, as most systems contain states that can only be an initial condition. Those states are generally called the *Garden of Eden* in cellular automata. The transition function's injectivity implies that for every $b \in \mathbb{B}^n$, there is at most one state that maps to it. Because the state space is finite, they are therefore equivalent. We have the following two important propositions linking bijectivity and some property of the transition function.

Proposition A.3. *Bijectivity of the transition function τ implies $\tau(\overrightarrow{\text{True}}) = \overrightarrow{\text{True}}$.*

Proof. We will prove this proposition by contradiction. By assumption, the transition τ function is bijective. As a result, among the 2^n possible states, $\overrightarrow{\text{False}}$ maps to itself, and the remaining $2^n - 1$ vectors must be mapped onto by exactly one other vector. Hence, the image of the transition function must contain all Boolean vectors in \mathbb{B}^n , such that each index i in the transition function's image contains 2^{n-1} True and 2^{n-1} False. We use a counting argument to prove that it is impossible for the image of the transition function to simultaneously map $\tau(\overrightarrow{\text{True}}) \neq \overrightarrow{\text{True}}$ while possessing the necessary number of True and False entries.

First, for Boolean vectors $a_k, a_l \in \mathbb{B}^n$, we define a convenient set of valid pairs $P = \{(a_k, a_l)\}$ such that $a_l = \neg a_k$. The pairs in this set have the convenient

property that $a_k \vee a_l = \overrightarrow{\text{True}}$, and $a_k \wedge a_l = \overrightarrow{\text{False}}$. We call such pairs *complementary valid pairs*. Because each vector a_k has precisely one negation $\neg a_k$, for 2^n vectors, there are 2^{n-1} complementary valid pairs.

Next, we make explicit that $(\overrightarrow{\text{False}}, \overrightarrow{\text{True}})$ is a complementary valid pair. Now let us assume that, while $\tau(\overrightarrow{\text{False}}) = \overrightarrow{\text{False}}$, we have $\tau(\overrightarrow{\text{True}}) = c \neq \overrightarrow{\text{True}}$. Hence, there must exist an index i for which the i -th element of c , c_i , is False.

The existence of $c_i = \text{False}$ is what generates the contradiction. Specifically, recall that the complementary valid pairs must satisfy Proposition A.1 such that

$$\sigma'(\tau(a_k)) \oplus \sigma'(\tau(a_l)) \approx \sigma'(c).$$

If we consider only the i -th index of this relation, we have

$$\sigma'(\tau(a_k))_i \oplus \sigma'(\tau(a_l))_i \approx \sigma'(c)_i \in \{-\}. \quad (\text{A6})$$

Based on the operator \oplus , the only way to form a negative result in the i -th index is for either or both of the terms on the left-hand side to be negative, which requires that at least one of $\tau(a_k)_i$ or $\tau(a_l)_i$ be False.

Hence, in the image of each complementary valid pair $(\tau(a_k), \tau(a_l))$, the i -th element of at least one must be False, such that we require at least 2^{n-1} Falses across all complementary valid pairs. Initially, it appears that there may be precisely enough Falses, because the bijectivity of the transition function requires 2^{n-1} True and 2^{n-1} False elements at index i . However, the valid pair $(\overrightarrow{\text{False}}, \overrightarrow{\text{True}})$ actually uses *two* of these Falses at index i , because $\tau(\overrightarrow{\text{False}})_i = \text{False}$, and $\tau(\overrightarrow{\text{True}})_i = c_i = \text{False}$.

In summary, we assume that τ is a bijective transition function mapping $\tau(\overrightarrow{\text{True}}) \neq \overrightarrow{\text{True}}$. For the complementary valid pairs P , Proposition A.1 requires that there be at least 2^{n-1} False elements in the image of τ at index i . However, because the bijectivity of τ allows precisely 2^{n-1} False elements in the image of τ at index i , and the pair $(\overrightarrow{\text{False}}, \overrightarrow{\text{True}})$ takes two of them, we have a contradiction; therefore we need to have $\tau(\overrightarrow{\text{True}}) = \overrightarrow{\text{True}}$. □

Proposition A.4. *Let τ be a bijective transition function and let $(a, \neg a)$ be a complementary valid pair; then for all i either $\tau(a)_i = \text{false}$ or $\tau(\neg a)_i = \text{false}$.*

Proof. We will proceed by contradiction. Let $(a, \neg a)$ be a complementary valid pair; then by Proposition A.1 and Proposition A.3, we must have for each index i that

$$\sigma'(\tau(a))_i \oplus \sigma'(\tau(\neg a))_i \approx +.$$

There is three possible cases for that to happen:

1. $\tau(a)_i = \text{true}$ and $\tau(\neg a)_i = \text{true}$,
2. $\tau(a)_i = \text{true}$ and $\tau(\neg a)_i = \text{false}$,
3. $\tau(a)_i = \text{false}$ and $\tau(\neg a)_i = \text{true}$.

However, from bijectivity, we have that the i -th component of the image of τ must map to 2^{n-1} Trues and 2^{n-1} Falses. Hence, as in the previous proposition, we have a contradiction.

Specifically, because τ is bijective, every vector in $b \in \mathbb{B}^n$ appears precisely once in the image of τ . This allows us to create a contradiction for the first case. Let $\tau(a)_i = \text{true}$ and $\tau(-a)_i = \text{true}$. Then there are only $2^{n-1} - 2$ True values available in the image of τ . Since there are still $2^{n-1} - 1$ valid pairs, there is at least one pair $(b, -b)$, such that $\tau(b)_i = \text{false}$ and $\tau(-b)_i = \text{false}$ which is a contradiction with Proposition A.3. Therefore either $\tau(a)_i = \text{false}$ or $\tau(-a)_i = \text{false}$. \square

We are now equipped to answer one of our questions of interest with this property. Do long cycles become possible at some point? The task of proving that a cycle of a given length is impossible for a given n is not a trivial task, but there is a trivial path for the case 2^n and a relatively simple one for the case $2^n - 1$. We hope that these two proofs will shed some light on how someone could prove the smaller cases. We have the following proposition:

Proposition A.5. *For $n > 1$ there is no map τ such that $A \in \{-1, 0, 1\}^{n \times n}$ and with a maximum cycle length greater than or equal to $2^n - 1$.*

Proof. We will tackle both cases separately.

a. *case 2^n :* Because of the linearity of the map α we have that $\alpha(\iota(0 \in \mathbb{B}^n)) = 0$. Therefore, cycles of length 2^n are impossible.

b. *case $2^n - 1$:* For a cycle of length $2^n - 1$, we will proceed by contradiction. In this case, the transition function needs to be bijective since $\tau(\overrightarrow{\text{False}}) = \overrightarrow{\text{False}}$ and no two states can map to the same state. Since $\overrightarrow{\text{False}}$ cannot be part of the cycle, $\overrightarrow{\text{True}}$ needs to be part of it and cannot map to itself. Therefore, there exists an i such that $\tau(\overrightarrow{\text{True}})_i = \text{False}$, which is a contradiction of Proposition A.3, thereby precluding a $2^n - 1$ cycle. \square

This type of counting argument is our principal tool to prove propositions in this model. Computationally, it can be shown that no solution satisfies Proposition A.1 for cycles of length $2^n - 2$ for $n = 4$. In general, the proposition appears enough to determine what cycle lengths are impossible. However, it is challenging to construct a proof showing that a pair will break this property in every case.

The following propositions begin to solve the problem of reflection symmetry. In this paper, we consider two types of reflection symmetry. The first one is the partial reflection symmetry and is defined as follows:

Definition A.6. *The transition function τ is said to be partially reflection symmetric for the index i if and only if*

$$\forall b \in \mathbb{B}^n \quad \tau(b)_i = b'_i \Leftrightarrow \tau(-b)_i = -b'_i. \quad (\text{A7})$$

A completely reflection-symmetric transition function τ is a transition function that is partially reflection-symmetric for all $i \in 1, \dots, n$. A completely reflection-symmetric transition function has the property that opposite states always map to opposite states.

Remark A.7. *Complete reflection symmetry of a transition function τ implies that $\tau(\overrightarrow{\text{True}}) = \overrightarrow{\text{True}}$.*

Proof. The proof is rather straightforward since from the symmetry we have if $\tau(b) = b'$ then $\tau(-b) = -b'$. By replacing b by $\overrightarrow{\text{False}}$ and since we have for all dynamics $\tau(\overrightarrow{\text{False}}) = \overrightarrow{\text{False}}$,

$$\tau(\overrightarrow{\text{False}}) = \overrightarrow{\text{False}} \Rightarrow \tau(\overrightarrow{\text{True}}) = \overrightarrow{\text{True}}.$$

\square

Though simple, this remark is nonetheless important in the sense that we can use a stricter condition asking for $\alpha(\iota(\overrightarrow{\text{True}})) = \overrightarrow{1}$ instead of $\tau(\overrightarrow{1}) = \overrightarrow{1}$ to characterize which transition function is a reflection-symmetric one. As we will see this condition is, in fact, equivalent to reflection symmetry. The difference between this condition and the previous one is that $\overrightarrow{\text{True}}$ can map under α to any vector containing only positive numbers for the first one. On the other hand, the second one can only map to the vector $\overrightarrow{1} \in \mathbb{Z}^n$. This condition means that the matrix A has column sums equal to 1. In a more model-oriented interpretation, this means that there is one more incoming excitation than inhibition. Surprisingly, the stricter condition is equivalent to the statement of being completely reflection-symmetric. This condition also appears when studying bijective transition functions. Before proving the full statement, let us first prove it in the forward direction.

Proposition A.8. *The condition $\alpha(\overrightarrow{1}) = \overrightarrow{1}$ implies a completely reflection-symmetric transition function τ .*

Proof. First, we provide the following relation in \mathbb{Z}^n for all $a \in \mathbb{B}^n$ for the not operator: $\iota(-a) = \overrightarrow{1} - \iota(a)$.

Let $\tau(a) = b$ with $a, b \in \mathbb{B}^n$ and let $\alpha(\overrightarrow{1}) = \overrightarrow{1}$, then by the definition of τ we have $\theta(\alpha(\iota(a))) = b$, and then

$$\begin{aligned} \tau(-a) &= \theta(\alpha(\iota(-a))) \\ &= \theta(\alpha(\overrightarrow{1} - \iota(a))) & \iota(-a) &= \overrightarrow{1} - \iota(a) \\ &= \theta(\alpha(\overrightarrow{1}) - \alpha(\iota(a))) & \text{linearity} \\ &= \theta(\overrightarrow{1} - \alpha(\iota(a))) & \text{assumption} \\ &= -\theta(\alpha(\iota(a))) \\ &= -b, \end{aligned}$$

where we used the fact that $\theta(\overrightarrow{1} - b) = -\theta(b)$, which is true for $b \in \mathbb{Z}^n$ and which is not true for the more general case $b \in \mathbb{R}^n$. \square

We can now prove the reverse direction of Proposition A.8 and show that reflection symmetry is equivalent to $\alpha(\vec{1}) = \vec{1}$.

Proposition A.9. *A transition function τ is reflection symmetric if and only if $\alpha(\vec{1}) = \vec{1}$.*

Proof. The first direction, which $\alpha(\vec{1}) = \vec{1}$ implies reflection symmetry has already been provided in Proposition A.8. The converse is also simple to prove by contradiction. Let $r_i(\alpha) = \sum_j A_{ij}$ be the column sum for a given α . We can divide the proof into three cases: the sum is greater than 1 for a given row i , equal to 1, or lower than 1. We only have to show that the lower and greater cases contradict the reflection symmetry hypothesis.

Let us first analyze how the vector $\alpha(\iota(b)) \in \mathbb{Z}^n$ is related to $\alpha(\iota(-b)) \in \mathbb{Z}^n$. For both case we have that

$$\begin{aligned} \alpha(\iota(-b))_i &= \alpha(\vec{1} - \iota(b))_i, \\ &= \alpha(\vec{1})_i - \alpha(\iota(b))_i, && \text{linearity} \\ &= r_i(\alpha) - \alpha(\iota(b))_i. && \text{def.} \end{aligned} \quad (\text{A8})$$

If there exists an i such that $r_i(\alpha) < 1$, then for $b = \vec{0}$ we have that $\alpha(\vec{1})_i = r_i(\alpha) \leq 0$ and therefore $\tau(\vec{1}) \neq \vec{1}$, which is in contradiction to Proposition A.7. Therefore we cannot have $r_i(\alpha) < 1$ and reflection symmetry at the same time.

For the other case, let $r_i(\alpha) > 1$. Then there are at least two elements in A_{ji} equal to 1 in the i -th column. One of them is at least not in row i . Call this row j , and hence we have $j \neq i$ and $\tau(\theta(e_j))_i = 1$. Then $\alpha(e_j)_i = 1$ since there is only one node activated by e_j . Because of our hypothesis of reflection symmetry, we have that $\alpha(-e_j)_i \leq 0$. However, using A8 we have that,

$$0 \geq \alpha(-e_j)_i = r_i(\alpha) - 1 \geq 1,$$

which is a contradiction. Therefore since i is arbitrary, we need $r_i(\alpha) = 1, \forall i$. \square

An exciting property of bijective transition functions is that they are all reflection-symmetric, which is formalized and proved in the following proposition.

Proposition A.10. *All bijective transition functions are completely reflection symmetric.*

Proof. With the tool presented earlier, this proposition is straightforward to prove and is simply a result of Proposition A.4. Specifically, a transition function is completely reflection symmetric if $\tau(a) = b$ implies $\tau(-a) = -b$. By proposition A.4, the set $(a, -a)$ is a complementary valid pair where each element i satisfies $\tau(a)_i = \neg\tau(-a)_i$. Because this relation must hold true across all elements i , we have that $\tau(a) = \neg\tau(-a)$, thereby satisfying the condition for complete reflection symmetry. \square

As seen in the proof above, the property $\alpha(\vec{1}) = \vec{1}$ also has a particular relation with bijectivity. We have

shown that reflection-symmetric transition functions necessitate that the number of incoming excitatory edges be one more than the number of incoming inhibitory edges. We can ask if there is a similar property for the opposite condition. What if all nodes have one more outgoing excitatory edge than the number of inhibitory edges? This condition is, unsurprisingly, connected to bijectivity; however, before trying to understand this connection, we need to understand how bijectivity appears. We, therefore, need a notion similar to linear dependency but tailored to our threshold operator θ . We call this type of dependence θ -dependence.

Definition A.11. *A set S of vectors in $\{-1, 0, 1\}^n$ is θ -dependent if there exist two subsets $A, B \subset S$ such that $A \neq B$ where one can be empty such that*

$$\theta\left(\sum A\right) = \theta\left(\sum B\right). \quad (\text{A9})$$

If there exists no such set, then we will call the set S θ -independent.

We have the following property.

Proposition A.12. *Let I be the collection of all θ -independent sets S in $2^{\{-1, 0, 1\}^n}$. Then I is an independence system as defined in [59] but not a matroid.*

Both matroid and independence systems share the property that I needs to include the empty set, which is true by definition for θ -independence. They also share the property that if $S \subset I$, then all $S' \subset S$ are also in I . By definition, this is also true for the θ -independence relation. On the other hand, θ -independence does not imply, as for linear independence, the independent set exchange property, which can be stated as: Let A and B be two independent sets and let $|A| > |B|$. Then the independent set exchange property implies that there exists an $a \in A \setminus B$ such that $B \cup a$ is independent.

To show that (\mathbb{R}^n, I) is not a matroid, we only need to give a counterexample. For example let $A = (1, 0), (0, 1)$ and let $B = \{(1, 1)\}$. Then clearly adding any element of A in B will lead to a dependent set. One could also wonder how this type of dependency is related to linear dependency. The first question one can ask is, Are linearly independent subsets of $2^{\{-1, 0, 1\}^n}$ also θ -independent? Unfortunately the answer is no. For example, the subset $\{(-1, 1), (1, 1)\}$ is linearly independent but it is not θ -independent since $A = \{(-1, 1)\}$ and $B = \{(-1, 1), (1, 1)\}$ both map to $(0, 1)$ under θ .

On the other hand, at least for $n \leq 4$, θ -independence implies linear independence. Unfortunately, we were unable to find a satisfying proof for all n . We, therefore, can only conjecture this property.

Conjecture A.13. *θ -independence implies linear independence.*

The importance of the concept of θ -independence comes from the following proposition.

TABLE I. Maximal θ -independent sets for n from 1 to 4.

n	# θ -indep. sets	maximal θ -indep. sets
1	1	{ (1) }
2	6	{ (1,0),(0,1) }
3	60	{ (1,0,0),(0,0,1),(0,1,0) }, { (1,1,-1),(1,-1,1),(-1,1,1) }
4	1169	{ (0,0,0,1),(0,1,0,0),(0,0,1,0),(1,0,0,0) }, { (0,0,0,1),(-1,1,1,0),(1,1,-1,0),(1,-1,1,0) }, { (0,1,1,-1),(1,0,0,0),(0,-1,1,-1),(0,1,-1,1) }, { (-1,0,1,1),(0,1,0,0),(1,0,1,-1),(1,0,-1,1) }, { (0,0,1,0),(1,-1,0,1),(1,1,0,-1),(-1,1,0,1) }

Proposition A.14. *There is a surjection from the set of bijective transition functions of n nodes to the set of θ -independent sets for n nodes of cardinality n .*

Proof. The proof comes from the fact that any ordering of an n -element θ -independent set can be regarded as a matrix where each column is the set's ordered vector. Therefore, from whichever θ -independent set, there exists $n!$ matrices generating bijective transition functions. The bijectivity of the transition functions comes directly from the θ -independence. Finally, every matrix producing bijective dynamics has a set of columns that is necessarily θ -independent since the multiplication by a binary vector is equivalent to summing a subset of the columns. \square

For $n \leq 4$, all bijective networks share the property that the column sum equals 1. For $n > 4$, a complete sampling of the design space is impossible. However, using random searches we never found a bijective transition function where the column did not sum to 1. Yet the converse is definitively false; a matrix with row sum and column sum equal to 1 is not necessarily bijective. A simple counterexample can be found for $n = 4$:

$$A = \begin{bmatrix} -1 & 1 & 1 & 0 \\ 1 & -1 & 1 & 0 \\ 1 & 0 & -1 & 1 \\ 0 & 1 & 0 & 0 \end{bmatrix}.$$

The matrix A leads to a dynamic where $(0, 1, 1, 1)$ and $(0, 1, 1, 0)$ both map to $(1, 0, 0, 1)$. This property, if true, has a similar interpretation to the row sum condition for symmetric matrices, but for bijectivity, it is the ratio of excitation to inhibition of outgoing edges that matters. Therefore it seems that there is a link between bijectivity and the concept of generalized doubly stochastic matrices [60, 61]. Such matrices, in some cases, follow a generalized Birkhoff's theorem [62] which implies that they can be expressed as a sum of permutation matrices. This connection could explain the link between the two properties, which motivates us to conjecture the two following statements:

Conjecture A.15. *A bijective and valid transition function will have a column sum of 1.*

Conjecture A.16. *Bijectivity of valid transition functions is equivalent to having row and column sums equal to 1.*

TABLE II. Maximal θ -independent sets for n from 1 to 4.

n	length	matrices
2	2	$\begin{bmatrix} -1 & 1 \\ 0 & 1 \end{bmatrix}$ $\begin{bmatrix} -1 & 1 \\ 1 & -1 \end{bmatrix}$ $\begin{bmatrix} -1 & 1 \\ 1 & 0 \end{bmatrix}$ $\begin{bmatrix} -1 & 1 \\ 1 & 1 \end{bmatrix}$ $\begin{bmatrix} 0 & 1 \\ 1 & 0 \end{bmatrix}$
3	6	$\begin{bmatrix} 1 & -1 & 1 \\ 1 & 1 & -1 \\ -1 & 1 & 1 \end{bmatrix}$
4	10	$\begin{bmatrix} -1 & 0 & 1 & 1 \\ 0 & 0 & 0 & 1 \\ 0 & 1 & 0 & 0 \\ 1 & -1 & 1 & 0 \end{bmatrix}$, $\begin{bmatrix} 0 & -1 & 1 & 1 \\ 1 & 0 & 0 & 0 \\ 0 & 1 & 0 & 1 \\ 0 & 1 & -1 & 1 \end{bmatrix}$

The property also seems to be related to a monotone matrix's property (in the sense of Collatz) as defined in [63]. A monotone matrix A has the property that its inverse contains only positive numbers. Monotonicity is also equivalent to the proposition: if for all $v \in \mathbb{R}^n$, $Av \geq 0$ implies $v \geq 0$ with \geq taken element-wise. For $n \leq 4$, monotonicity implies bijectivity, and for $n > 5$, we did not find any matrix suggesting the opposite.

-
- [1] H. Chen, G. Wang, R. Simha, C. Du, and C. Zeng, Boolean models of biological processes explain cascade-like behavior, *Scientific reports* **6**, 1 (2016).
- [2] A. Berdahl, A. Shreim, V. Sood, M. Paczuski, and J. Davidsen, Random sampling versus exact enumeration of attractors in random boolean networks, *New Journal of Physics* **11**, 043024 (2009).
- [3] K. Iguchi, S.-i. Kinoshita, and H. S. Yamada, Boolean dynamics of kauffman models with a scale-free network, *Journal of theoretical biology* **247**, 138 (2007).
- [4] S. Sinha, B. M. Jones, I. M. Traniello, S. A. Bukhari, M. S. Halfon, H. A. Hofmann, S. Huang, P. S. Katz, J. Keagy, V. J. Lynch, *et al.*, Behavior-related gene regulatory networks: A new level of organization in the brain, *Proceedings of the National Academy of Sciences* **117**, 23270 (2020).
- [5] K. Klemm and S. Bornholdt, Topology of biological networks and reliability of information processing, *Proceedings of the National Academy of Sciences* **102**, 18414 (2005).
- [6] D. B. Forger, *Biological clocks, rhythms, and oscillations: the theory of biological timekeeping*, Vol. - (MIT Press, 2017) pp. -.
- [7] T. Kobayashi, H. Mizuno, I. Imayoshi, C. Furusawa, K. Shirahige, and R. Kageyama, The cyclic gene *hes1* contributes to diverse differentiation responses of embryonic stem cells, *Genes & development* **23**, 1870 (2009).
- [8] D.-G. Wang, S. Wang, B. Huang, and F. Liu, Roles of cellular heterogeneity, intrinsic and extrinsic noise in variability of p53 oscillation, *Scientific reports* **9**, 1 (2019).
- [9] M. S. Nash, K. W. Young, R. J. Challiss, and S. R. Nahorski, Receptor-specific messenger oscillations, *Nature* **413**, 381 (2001).
- [10] J. Aracena, Maximum number of fixed points in regulatory boolean networks, *Bulletin of mathematical biology* **70**, 1398 (2008).
- [11] F. Mori and A. Mochizuki, Expected number of fixed points in boolean networks with arbitrary topology, *Physical review letters* **119**, 028301 (2017).
- [12] J. Aracena, A. Richard, and L. Salinas, Number of fixed points and disjoint cycles in monotone boolean networks, *SIAM Journal on Discrete Mathematics* **31**, 1702 (2017).
- [13] A. Raj and A. Van Oudenaarden, Nature, nurture, or chance: stochastic gene expression and its consequences, *Cell* **135**, 216 (2008).
- [14] L. Chen, D. Kulasiri, and S. Samarasinghe, A novel data-driven boolean model for genetic regulatory networks, *Frontiers in physiology* **9**, 1328 (2018).
- [15] C. Campbell and R. Albert, Stabilization of perturbed boolean network attractors through compensatory interactions, *BMC systems biology* **8**, 1 (2014).
- [16] S. Coppersmith, L. P. Kadanoff, and Z. Zhang, Reversible boolean networks i: distribution of cycle lengths, *Physica D: Nonlinear Phenomena* **149**, 11 (2001).
- [17] W. Z. Ouma, K. Pogacar, and E. Grotewold, Topological and statistical analyses of gene regulatory networks reveal unifying yet quantitatively different emergent properties, *PLoS computational biology* **14**, e1006098 (2018).
- [18] B. Drossel, T. Mihaljev, and F. Greil, Number and length of attractors in a critical kauffman model with connectivity one, *Physical Review Letters* **94**, 088701 (2005).
- [19] Z. Somogyvari and S. Payrits, Length of state cycles of random boolean networks: an analytic study, *Journal of Physics A: Mathematical and General* **33**, 6699 (2000).
- [20] S. Mangan and U. Alon, Structure and function of the feed-forward loop network motif, *Proceedings of the National Academy of Sciences* **100**, 11980 (2003).
- [21] Y. Zhang, Q. Ouyang, and Z. Geng, Topological origin of global attractors in gene regulatory networks, *Science China Physics, Mechanics & Astronomy* **58**, 1 (2015).
- [22] G. Wang, C. Du, H. Chen, R. Simha, Y. Rong, Y. Xiao, and C. Zeng, Process-based network decomposition reveals backbone motif structure, *Proceedings of the National Academy of Sciences* **107**, 10478 (2010).
- [23] F. Li, T. Long, Y. Lu, Q. Ouyang, and C. Tang, The yeast cell-cycle network is robustly designed, *Proceedings of the National Academy of Sciences* **101**, 4781 (2004).
- [24] F. Bridoux, C. Gaze-Maillet, K. Perrot, and S. Sené, Complexity of limit-cycle problems in boolean networks, in *International Conference on Current Trends in Theory and Practice of Informatics* (Springer, 2021) pp. 135–146.
- [25] E. Bullmore and O. Sporns, The economy of brain network organization, *Nat Rev Neurosci* **13**, 336 (2012).
- [26] G. Wu, Q. Yan, J. A. Jones, Y. J. Tang, S. S. Fong, and M. A. G. Koffas, Metabolic burden: Cornerstones in synthetic biology and metabolic engineering applications, *Trends Biotechnol* **34**, 652 (2016).
- [27] J. G. Zañudo and R. Albert, An effective network reduction approach to find the dynamical repertoire of discrete dynamic networks, *Chaos* **23**, 025111 (2013).
- [28] R. Egger, Y. Tupikov, M. Elmaleh, K. A. Katlowitz, S. E. Benezra, M. A. Picardo, F. Moll, J. Kornfeld, D. Z. Jin, and M. A. Long, Local axonal conduction shapes the spatiotemporal properties of neural sequences, *Cell* **183**, 537 (2020).
- [29] J. Jaeger and A. Crombach, Life's attractors: understanding developmental systems through reverse engineering and in silico evolution, *Adv Exp Med Biol* **751**, 93 (2012).
- [30] H. Yamamoto, S. Moriya, K. Ide, T. Hayakawa, H. Akima, S. Sato, S. Kubota, T. Tanii, M. Niwano, S. Teller, J. Soriano, and A. Hirano-Iwata, Impact of modular organization on dynamical richness in cortical networks, *Sci Adv* **4**, eaau4914 (2018).
- [31] A. Naldi, C. Hernandez, W. Abou-Jaoudé, P. T. Monteiro, C. Chaouiya, and D. Thieffry, Logical modeling and analysis of cellular regulatory networks with ginsim 3.0, *Frontiers in physiology* **9**, 646 (2018).
- [32] H. Klarner, A. Streck, and H. Siebert, Pyboolnet: a python package for the generation, analysis and visualization of boolean networks, *Bioinformatics* **33**, 770 (2017).
- [33] S. M. Shaffer, M. C. Dunagin, S. R. Torborg, E. A. Torre, B. Emert, C. Krepler, M. Beqiri, K. Sproesser, P. A. Brafford, M. Xiao, *et al.*, Rare cell variability and drug-induced reprogramming as a mode of cancer drug resistance, *Nature* **546**, 431 (2017).
- [34] Z. Burda, A. Krzywicki, O. C. Martin, and M. Zagorski, Motifs emerge from function in model gene regulatory networks, *Proceedings of the National Academy of Sciences* **108**, 17263 (2011).
- [35] Z. Zhang, W. Ye, Y. Qian, Z. Zheng, X. Huang, and G. Hu, Chaotic motifs in gene regulatory networks, *Plos*

- one **7**, e39355 (2012).
- [36] S. Hossein, M. D. Reichl, and K. E. Bassler, Symmetry in critical random boolean network dynamics, *Physical Review E* **89**, 042808 (2014).
- [37] R. E. Stearns, S. Ravi, M. V. Marathe, and D. J. Rosenkrantz, Symmetry properties of nested canalizing functions, *Discrete Mathematics & Theoretical Computer Science* **21** (2019).
- [38] F. Morone, I. Leifer, and H. A. Makse, Fibration symmetries uncover the building blocks of biological networks, *Proceedings of the National Academy of Sciences* **117**, 8306 (2020).
- [39] I. Leifer, F. Morone, S. D. Reis, J. S. Andrade Jr, M. Sigman, and H. A. Makse, Circuits with broken fibration symmetries perform core logic computations in biological networks, *PLoS computational biology* **16**, e1007776 (2020).
- [40] Y. Cantor, B. Khan, and K. Dombrowski, Towards a formal understanding of bateson’s rule: Chromatic symmetry in cyclic boolean networks and its relationship to organism growth and cell differentiation, *Procedia Computer Science* **36**, 476 (2014).
- [41] M. Liu and K. E. Bassler, Emergent criticality from co-evolution in random boolean networks, *Physical Review E* **74**, 041910 (2006).
- [42] P. Chatterjee and R. M. Werner, Gender disparity in citations in high-impact journal articles, *JAMA Netw Open* **4**, e2114509 (2021).
- [43] J. M. Fulvio, I. Akinola, and B. R. Postle, Gender (im)balance in citation practices in cognitive neuroscience, *J Cogn Neurosci* **33**, 3 (2021).
- [44] J. D. Dworkin, K. A. Linn, E. G. Teich, P. Zurn, R. T. Shinohara, and D. S. Bassett, The extent and drivers of gender imbalance in neuroscience reference lists, *Nature Neuroscience* **23**, 918 (2020).
- [45] M. A. Bertolero, J. D. Dworkin, S. U. David, C. L. Lloreda, P. Srivastava, J. Stiso, D. Zhou, K. Dzirasa, D. A. Fair, A. N. Kaczkurkin, B. J. Marlin, D. Shohamy, L. Q. Uddin, P. Zurn, and D. S. Bassett, Racial and ethnic imbalance in neuroscience reference lists and intersections with gender, *bioRxiv* (2020).
- [46] E. G. Teich, J. Z. Kim, C. W. Lynn, S. C. Simon, A. A. Klishin, K. P. Szymula, P. Srivastava, L. C. Bassett, P. Zurn, J. D. Dworkin, and D. S. Bassett, Citation inequity and gendered citation practices in contemporary physics, *arXiv* **2112**, 09047 (2021).
- [47] X. Wang, J. D. Dworkin, D. Zhou, J. Stiso, E. B. Falk, D. S. Bassett, P. Zurn, and D. M. Lydon-Staley, Gendered citation practices in the field of communication, *Annals of the International Communication Association* **1**, 10.1080/23808985.2021.1960180 (2021).
- [48] M. L. Dion, J. L. Sumner, and S. M. Mitchell, Gendered citation patterns across political science and social science methodology fields, *Political Analysis* **26**, 312 (2018).
- [49] S. M. Mitchell, S. Lange, and H. Brus, Gendered citation patterns in international relations journals, *International Studies Perspectives* **14**, 485 (2013).
- [50] D. Maliniak, R. Powers, and B. F. Walter, The gender citation gap in international relations, *International Organization* **67**, 889 (2013).
- [51] N. Caplar, S. Tacchella, and S. Birrer, Quantitative evaluation of gender bias in astronomical publications from citation counts, *Nature Astronomy* **1**, 0141 (2017).
- [52] D. Zhou, E. J. Cornblath, J. Stiso, E. G. Teich, J. D. Dworkin, A. S. Blevins, and D. S. Bassett, Gender diversity statement and code notebook v1.0 (2020).
- [53] G. Sood and S. Laohaprapanon, Predicting race and ethnicity from the sequence of characters in a name, *arXiv preprint arXiv:1805.02109* **1** (2018).
- [54] K. Deb, A. Pratap, S. Agarwal, and T. Meyarivan, A fast and elitist multiobjective genetic algorithm: Nsga-ii, *IEEE transactions on evolutionary computation* **6**, 182 (2002).
- [55] J. J. Hopfield, Neural networks and physical systems with emergent collective computational abilities, *Proceedings of the national academy of sciences* **79**, 2554 (1982).
- [56] J. J. Hopfield, Hopfield network, *Scholarpedia* **2**, 1977 (2007).
- [57] S. Montagna, M. Braccini, and A. Roli, The impact of self-loops on boolean networks attractor landscape and implications for cell differentiation modelling, *IEEE/ACM transactions on computational biology and bioinformatics* **1**, 1 (2020).
- [58] M. Braccini, S. Montagna, and A. Roli, Self-loops favour diversification and asymmetric transitions between attractors in boolean network models, in *Italian Workshop on Artificial Life and Evolutionary Computation*, Vol. 1 (Springer, 2018) pp. 30–41.
- [59] J. A. Bondy and U. S. R. Murty, *Graph theory*, volume 244 of, *Graduate texts in Mathematics* **623** (2008).
- [60] H. Chiang and C.-K. Li, Generalized doubly stochastic matrices and linear preservers, *Linear and Multilinear Algebra* **53**, 1 (2005).
- [61] H.-C. Lai, On the linear algebra of generalized doubly stochastic matrices and their equivalence relations and permutation basis, *Japan Journal of Applied Mathematics* **3**, 357 (1986).
- [62] S.-J. Cho and Y.-S. Nam, Convex polytopes of generalized doubly stochastic matrices, *Communications of the Korean Mathematical Society* **16**, 679 (2001).
- [63] O. Mangasarian, Characterizations of real matrices of monotone kind, *SIAM Review* **10**, 439 (1968).